https://doi.org/10.1016/j.jsv.2015.04.027

Statistical Enhancement of A Local Dynamic Equilibrium-based Damage Identification Strategy: *Theory and Experimental Validation*

Hao XU[1,2], Bo LU[2], Zhongqing SU[1,2†], and Li CHENG[1,2]

[1]The Hong Kong Polytechnic University Shenzhen Research Institute

Shenzhen 518057, P. R. China

[2]The Department of Mechanical Engineering, The Hong Kong Polytechnic University

Kowloon, Hong Kong SAR

Submitted to *Journal of Sound and Vibration*

(initially submitted on 7th January 2015; revised and re-submitted on 10th April 2015)

† To whom correspondence should be addressed
Email: MMSU@polyu.edu.hk (Prof. Zhongqing SU, *Ph.D.*), Tel : +852-2766-7818

Abstract

A previously developed damage identification strategy, named *Pseudo–Excitation* (PE), was enhanced using a statistical processing approach. In terms of the local dynamic equilibrium of the structural component under inspection, the distribution of its vibration displacements, which are of necessity to construct the damage index in the PE, was re-defined using sole dynamic strains based on the statistical method. On top of those advantages inheriting from the original PE compared with traditional vibration-based damage detection including the independence of baseline signals and pre-developed benchmark structures, the enhanced PE (EPE) possesses improved immunity to the interference of measurement noise. Moreover, the EPE can facilitate practical implementation of online structural health monitoring, benefiting from the use of sole strain information. Proof-of-concept numerical study was conducted to examine the feasibility and accuracy of the EPE, and the effectiveness of the proposed statistical enhancement in re-constructing the vibration displacements was evaluated under noise influence; experimental validation was followed up by characterizing multi-cracks in a beam-like structure, in which the dynamic strains were measured using Lead zirconium titanate (PZT) sensors. For comparison, the original PE, the Gapped Smoothing Method (GSM), and the EPE were respectively used to evaluate the cracks. It was observed from the damage identification results that both the GSM and EPE were able to achieve higher identification accuracy than the original PE, and the robustness of the EPE in damage identification was proven to be superior than that of the GSM.

***Keywords*:** dynamic equilibrium; damage detection; statistical enhancement; strain measurement; structural health monitoring

1. Introduction

Relying on the examination of local dynamic equilibrium for different structural components, e.g., beam and plate component, the *Pseudo–excitation* (PE) method for damage identification was developed in recent studies [1-3]. Compared with conventional vibration-based damage detection methods established based on the changes in structural global vibration signature, e.g., eigen-frequency [4-7], mode shape [8,9], flexibility matrix [10,11] and damping property [12], the PE was able to identify structural damage in the absence of a variety of prerequisites that are of necessity for the conventional methods, such as baseline signal, benchmark structure, and the prior knowledge of structural boundary conditions [1], etc.

The effectiveness of the PE approach, however, was limited by several drawbacks. First, involving the high-order derivatives of vibration signals, the damage index of the PE was highly sensitive to the influence of measurement noise, and the captured signals can be severely contaminated by the noise, obscuring damage-associated signal features. On the other hand, because the original PE was applied by using the signal of vibration displacements, its application was largely limited to off-line damage identification due to the restrictions in the size and type of available displacement sensors. In the previous studies, scanning laser vibrometer (SLV) was adopted to measure the vibration displacements under the steady vibration state of inspected structure. Although with remarkable precision, the measurement using SLV, typified by point-wise scanning [13,14], was not able to fulfill the real-time reflection of ambient vibrations that are associate with structural operational state.

Measurement of dynamic strains has been widely adopted in a variety of methods for structural health monitoring [15-19]. Benefiting from the flexible selection of a wide range of types of strain sensors, e.g., impedance strain gauges, PZT and Fiber Bragg Grating (FBG) sensors, the on-line monitoring of structural health can be implemented cost-effectively. More importantly, for the PE, measured strain (curvature) signal involves largely reduced influence from measurement noise, compared with the curvature signals that constructed based on the second-order derivation of measured vibration displacements. However, because vibration displacements are of necessity to be included in the formulation of the damage index of the PE, an effective way must be developed to re-construct the distribution of vibration displacements depending on the signal of dynamic strains/curvatures, if sole strain information is used. Up to the present, however, only a very limited number of studies have been reported.

In this study, the original PE was enhanced to be applied based on the measurement of structural dynamic strains. The essence of the method resides on the re-construction of vibration displacements using measured strain/curvature signal, according to a statistical approach linked with the condition of structural local dynamic equilibrium. The EPE inherits the various advantages of the original PE, i.e., independence of baseline signal and benchmark structure, etc., and possesses improved noise immunity compared with the original PE. Moreover, relying on an explicit physical implication, the EPE is possible to show superior adaptability and robustness in damage identification compared with other benchmark-free methods, such as the GSM [20,21], developed based on conventional curvature mode shape [22,23] method.

Proof-of-concept numerical study was conducted to specify the implementation of the EPE, and the influence from measurement noise, with different levels, on the accuracy of damage identification was discussed. An experiment was carried out subsequently to characterize multi-cracks in a beam-like structure. PZT sensors were selected to measure the dynamic strains of the structure, and the vibration displacements were also measured using a SLV. The effectiveness of the proposed statistical approach for displacement re-construction was examined both numerically and experimentally. And the identification results constructed using three different methods, i.e., the original PE, the GSM, and the EPE, were presented and compared.

2. Enhanced PE (EPE) Method

2.1 Theory

Damage index of the original PE can be established based on equations of motion for different types of structural components, e.g., beam, plate or shell component. Using a homogeneous isotropic Euler-Bernoulli beam component as an example, the damage index, corresponding to steady vibration state, can be expressed as

$$\mathrm{DI}(x) = \left| EI \frac{\mathrm{d}^4 w(x)}{\mathrm{d}x^4} - \rho S \omega^2 w(x) \right|, \qquad \textbf{(1a)}$$

where $w(x)$ is the vibration displacement at location x; ω is the angular vibration frequency of the beam; E, ρ, I and S are the modulus of elasticity, density, cross-sectional moment of inertia and area of the beam under pristine statue, respectively. In classic beam vibration theory, $\mathrm{DI}(x)$ represents the distribution of external excitation on the surface of the beam without damage existence, and $\mathrm{DI}(x) = 0$ signifies the absence of external excitation. In a damaged beam, however, variations of $\mathrm{DI}(x)$ from zero can be

observed at the location of damage, particularly at the boundaries of damaged zone, where prominent singularities of $\mathrm{DI}(x)$ are formed due to the discontinuities of structural geometry and material, which can be well utilized to accurately indicate the location and size of damage. Because of the similarity between damage and actual excitation in causing variation in $\mathrm{DI}(x)$, the $\mathrm{DI}(x)$ in Eq. (1a), when used for damage identification, is defined as "*Pseudo–excitation*" (PE).

It should be emphasized that besides the singularities of $\mathrm{DI}(x)$ for locating damage, as explained above, the $\mathrm{DI}(x)$ signal always remain zero at the intact regions of tested structure because of the satisfaction of dynamic equilibrium therein. This feature further increases the accuracy of damage identification, and enables the PE to be applied with strong adaptability, for example, in the absence of baseline signal, benchmark structure, and the prior knowledge of structural boundary conditions.

The formulation of the damage index of the PE, as shown in Eq. (1a), can be easily derived for other structural components, for example, a two-dimensional damage index can be derived based on plate vibration theory, as

$$\mathrm{DI}(x,y) = \left| D\nabla^4 w(x,y) - \rho h\omega^2 w(x,y) \right| , \qquad \textbf{(1b)}$$

where D, of being $Eh^3/12(1-\nu^2)$, signifies the bending stiffness of the plate component; $w(x,y)$ is the vibration displacement; h and ν are the thickness and the Poisson's ratio, respectively.

Damage indices constructed according to Eq. (1a) and (1b) correspond to structures with isotropic material properties, e.g., metal, and damage index with different form is needed

to be established for structures with more complex material properties, such as composite structure, for which the condition of local dynamic equilibrium should be established using delamination theory. Moreover, in engineering practice, the surfaces of tested structures are usually not smooth, for example, stiffened composite plate. Under such circumstance, the non-smooth parts (e.g., the stiffeners) can still be detected as added masses and reflected by the damage indices of PE, because the PE is able to reveal any local change of geometric and material properties.

Characterized by fourth-order derivatives of vibration displacements, as included in Eq. (1a) and (1b), the PE suffers from the influence of measurement noise, because the noise influence contained in the vibration displacements, although with a small level, can be drastically amplified due to the high-order derivation [1]. Aimed at noise reduction, the order of the derivative of vibration signals can be reduced based on the direct measurement of curvature (strain) signal. The formulation of the original PE is modified, using beam component as an example, by dividing $\rho S\omega^2$ on both the left- and right-side terms of Eq. (1a), leading to the damage index of the EPE as

$$\mathrm{EDI}(x) = \left|\alpha\,\Phi_{\kappa}(x) - w_{\kappa}(x)\right|, \tag{2a}$$

where

$$\mathrm{EDI}(x) = \frac{\mathrm{DI}(x)}{\rho S\omega^2}\ ,\ \alpha = \frac{EI}{\rho S\omega^2}\ \text{and}\ \ \Phi_{\kappa}(x) = \frac{\mathrm{d}^2\kappa(x)}{\mathrm{d}x^2}, \tag{2b}$$

and

$$\kappa(x) = \frac{\mathrm{d}^2 w_{\kappa}(x)}{\mathrm{d}x^2}. \tag{2c}$$

In the above equations, $\kappa(x)$ is the curvature of vibration displacement, proportional to strain signal measured along *x* direction; $w_{\kappa}(x)$ represents the vibration displacement re-

constructed using $\kappa(x)$. $\mathrm{EDI}(x)$ is proportional to $\mathrm{DI}(x)$, as shown in Eq. (2b), thus is with equivalent accuracy of damage identification compared with $\mathrm{DI}(x)$ as shown in Eq. (1a).

With given geometric and material parameters and measured curvature (strain) signals, α and $\Phi_{\kappa}(x)$ in Eq. (2b) can be easily calculated. Thus the key step of constructing $\mathrm{EDI}(x)$ in Eq. (2a) resides on the re-construction of $w_{\kappa}(x)$ using $\kappa(x)$. By observing Eq. (2c), it is seen that $w_{\kappa}(x)$ can be derived through integrating $\kappa(x)$ in spatial domain, as introduced as follows.

2.2 Re-construction of Vibration Displacements Based on Curvature/Strain Signal

In practical application, the values of $\kappa(x)$ are measured discretely along tested structure. Corresponding to *m* measurement points located at $x_i\,(i=1,2,...m)$, $\kappa(x)$ can be expressed discretely as $\kappa(x_i)$. Normally, there is no explicit analytical expression for the distribution of $\kappa(x_i)$. But the distribution of $\kappa(x_i)$ can be approximated using curve fitting, expressed as

$$\kappa_{fit}(x_i) \approx \kappa(x_i), \tag{3}$$

where the values of $\kappa_{fit}(x_i)$ are extracted from the function of $\kappa_{fit}(x)$ which can be expressed as the summation of a series of integrable functions, e.g., polynomials.

The integral of $\kappa(x)$ is then approximated by that of $\kappa_{fit}(x)$. The indefinite integral of $\kappa_{fit}(x)$ is

$$\int \kappa_{fit}(x)\mathrm{d}x = F(x) + A, \quad \textbf{(4a)}$$

and

$$\int\int \kappa_{fit}(x)\mathrm{d}x = G(x) + Ax + B, \quad \textbf{(4b)}$$

where $F(x)$ is the primitive function of $\kappa_{fit}(x)$; $G(x)$ is the primitive function of $F(x)$; *A* and *B* are constants with arbitrary values. According to Eq. (2c), it can be understood that $w_\kappa(x)$ can be approximated using the form of Eq. (4b), as

$$w_\kappa(x) \approx G(x) + Ax + B, \quad \textbf{(5)}$$

where *A* and *B* are fixed values, to be determined statistically according to structural local dynamic equilibrium.

Corresponding to $x_i\,(i = 1, 2, ...m)$, $\mathrm{EDI}(x)$ in Eq. (2a) is written as a vector comprising of $\mathrm{EDI}(x_i)$. Without damage existence, $\mathrm{EDI}(x_i) = 0$ at every x_i, because of the satisfaction of dynamic equilibrium at x_i, as explained previously. And Eq. (2a) can be written as

$$\alpha\,\Phi_\kappa(x_i) - w_\kappa(x_i) = 0. \quad (i = 1, 2, ...m) \quad \textbf{(6a)}$$

By substituting Eq. (5) into Eq. (6a), a set of equations is formed, as

$$\begin{cases} Ax_1 + B = \alpha\,\Phi_\kappa(x_1) - G(x_1) \\ Ax_2 + B = \alpha\,\Phi_\kappa(x_2) - G(x_2) \\ ... \\ Ax_m + B = \alpha\,\Phi_\kappa(x_m) - G(x_m). \end{cases} \quad \textbf{(6b)}$$

Since the number of equations (measurement points), i.e., *m*, is normally much larger than that of the unknowns (*A* and *B*), *A* and *B* can be calculated by solving any two of the above equations. Because of damage existence, not all equations in Eq. (6b) truly hold, and false values of *A* and *B* will be obtained if equations located at damaged zone (particularly at the boundaries of damaged zone where $\mathrm{EDI}(x_i)$ shows prominent singularities) are involved.

Under such circumstance, a number of pairs of *A* and *B* can be calculated by solving all the combinations of the above equations in Eq. (6b), by doing which *A* and *B* can be estimated statistically, by excluding the abnormal pairs of *A* and *B*, identified as outliers [24,25] that show large differences from other pairs. The total number of the combinations of equations (pairs of *A* and *B*) can be calculated to be $m!/[2\times(m-2)!]$.

In the following analysis, a more straightforward way of estimating *A* and *B* is developed, by defining

$$Y(x_i) = Ax_i + B \quad (i = 1, 2, ...m), \tag{7}$$

where $Y(x_i)$ is calculated at different x_i according to the right-side terms of the equations in Eq. (6b), and then plotted along with the variation of x_i. Because *A* and *B* are with fixed values, the curve of $Y(x_i)$, if plotted using the true values of *A* and *B*, should be a straight line with *A* and *B* as its slope and intercept, respectively. However, nonlinear distribution of $Y(x_i)$ will be observed due to the existence of abnormal pairs of *A* and *B*, associate with damage or measurement noise. Thus linear curve fitting was applied based on the data of $Y(x_i)$, giving rise to the estimated values of *A* and *B* nearest to the true values.

3. Numerical Validation

The feasibility of the EPE was demonstrated using a finite element (FE) model of a damaged cantilever beam. The accuracies of displacement re-construction and damage identification were examined using the model.

3.1 FE Model

Considering an Euler-Bernoulli cantilever beam with geometric and material properties listed in Table 1, and the beam was clamped at its left end as shown in Fig. 1. A FE model of the beam, with 550 beam elements evenly distributing across the beam length, was created using commercial FEM code ANSYS®. A harmonic point excitation of 1000 Hz was applied at $x = 10\,\text{mm}$ (referring to Fig.1 for the coordinate system). The beam bore a damaged zone spanning over the region of $[890\text{mm}, 910\text{mm}]$, which was simulated with a reduced Young's modulus by 50% of their original value of corresponding elements within the damaged zone. To avoid any singularity caused by the excitation, an inspection region of $[200\text{mm}, 1100\text{mm}]$ was pre-determined to exclude the vicinity of the excitation point.

The curvature values, i.e., $\kappa(x_i)$, were calculated using a central finite difference method [26] based on the signal of vibration displacements obtained based on FE analysis. In the following study, $\kappa(x_i)$ were extracted from 46 measurement points evenly distributing along the inspection region, as shown in Fig. 2(a). The uniform distance between adjacent measurement points, defined as Δ_κ, is 20mm.

3.2 Results of Damage Identification

The two terms included in $\text{EDI}(x)$, $\alpha\Phi_\kappa(x_i)$ and $w_\kappa(x_i)$ as shown in Eq. (2a), were constructed, respectively, based on $\kappa(x_i)$. $\Phi_\kappa(x_i)$ was calculated using Eq. (2b), according to the central difference scheme as

$$\Phi_\kappa(x_i) = \frac{1}{\Delta_\kappa^2}\left[\kappa(x_{i-1}) - 2\kappa(x_i) + \kappa(x_{i+1})\right]. \quad \textbf{(8)}$$

The distribution of $\alpha\Phi_\kappa(x_i)$ is presented in Fig. 2(b). Characterized by the second-order derivative of vibration signal (two orders lower than the fourth-order included in Eq. (1a)),

$\alpha\Phi_{\kappa}(x_i)$ shows singularity at the damage location, but prominent fluctuations of $\alpha\Phi_{\kappa}(x_i)$ are also observed at the intact regions of the beam, jeopardizing the accuracy and precision of damage identification.

To re-construct the distribution of $w_{\kappa}(x_i)$, the signal of $\kappa(x_i)$ was first approximated by curve fitting. Because the frequency of vibration is relatively high, i.e., between the 8th and 9th natural frequencies of the beam model, badly conditioned polynomials, involving significantly high degrees, appeared when adopted for curve fitting. Thus the curve fitting was implemented based on the summation of Fourier series, with the form of

$$\kappa_{fit}(x) = a_0 + \sum_{i=1}^{n}\left[a_i \cos i\tau x + b_i \sin i\tau x\right], \qquad \textbf{(9a)}$$

where a_0, a_i, b_i, and τ were mathematically determined using least-squares algorithms; n is the order of the Fourier series. Figure 2(a) shows the distribution of $\kappa_{fit}(x)$ by setting $n=4$.

The primitive function, $G(x)$, as presented in Eq. (4b), can be easily derived based on Eq. (9a), to be

$$G(x) = \frac{a_0}{2}x^2 - \frac{1}{(i\tau)^2}\sum_{i=1}^{n}\left[a_i \cos i\tau x + b_i \sin i\tau x\right]. \qquad \textbf{(9b)}$$

And the approximated distribution of $w_{\kappa}(x_i)$, referring to Eq. (5), can be expressed as

$$w_{\kappa}(x_i) \approx \frac{a_0}{2}x_i^2 - \frac{1}{(i\tau)^2}\sum_{i=1}^{n}\left[a_i \cos i\tau x_i + b_i \sin i\tau x_i\right] + Y(x_i). \qquad \textbf{(9c)}$$

Remember that $Y(x_i)$ includes two unknowns, i.e., A and B as shown in Eq. (7), to be determined according to structural local dynamic equilibrium. Keeping $n=4$ in Eq. (9a),

$Y(x_i)$ was calculated at different x_i according to Eq. (6b) and plotted in Fig. 3(a). As expected, the overall trend of $Y(x_i)$ is as a straight line, except three abnormal points distributing randomly around the damage location. Based on the data of $Y(x_i)$, A and B were estimated using linear curve fitting, as presented in Fig. 3(a). And with A and B estimated, $w_\kappa(x_i)$ can be re-constructed according to Eq. (9c). In Fig. 3(b), it can be seen that the re-constructed vibration displacements basically coincide with the true displacements calculated based on FE analysis.

Using the re-constructed $w_\kappa(x_i)$ in Fig. 3(b), the values of $\mathrm{EDI}(x_i)$ were calculated according to Eq. (2a) and presented in Fig. 4. Both the location and size of the damaged zone were accurately identified. Specifically, the damage-related feature included in $\alpha\Phi_\kappa(x_i)$, as shown in Fig. 2(b), was largely highlighted by eliminating all the fluctuations in $\alpha\Phi_\kappa(x_i)$ at the intact regions using the re-constructed $w_\kappa(x_i)$ in Fig. 3(b).

3.3 Influence from Measurement Noise

To simulate experimental condition with noise influence involved, the data of $\kappa(x_i)$ were numerically polluted according to

$$\kappa^{\mathrm{n}}(x_i) = \kappa(x_i)\cdot(1+\varepsilon_i), \tag{10}$$

where $\kappa^{\mathrm{n}}(x_i)$ is the noise-corrupted counterpart of $\kappa(x_i)$; ε_i a Gaussian random real number related to the magnitude of $\kappa(x_i)$. In the succeeding analysis, $\mu(\varepsilon_i)=0$, and $\sigma(\varepsilon_i)$ was set to be 1%, 3% and 5%, respectively (μ and σ signify the mathematical manipulation of calculating mean and standard deviation, respectively).

In Fig. 5(a), it can be observed that the re-constructed $w_\kappa(x_i)$ signals show insignificant sensitivities to the noise influence, although certain degree of magnitude variations were observed by comparing the re-constructed and true displacements. Corresponding to $\sigma(\varepsilon_i)=5\%$ in Eq. (10), the distribution of $Y(x_i)$ is plotted along with the variation of x_i, as presented in Fig. 5(b). It can be seen that although the data of $Y(x_i)$ distribute more randomly compared with that in Fig. 3(a) due to noise influence, *A* and *B* can still be estimated accurately by the linear curve fitting (shown in Fig. 5(b)), evidenced by the distributions of re-constructed displacements in Fig. 5(a). Compared with the re-constructed displacements, the signals of $\alpha\,\Phi_\kappa(x_i)$ are more vulnerable to noise influence, showing random fluctuations at the intact regions of the beam model, as presented in Fig. 6(a), (c) and (e), respectively. The reason is attributed to the involvement of second-order derivation of $\kappa(x_i)$ in $\alpha\,\Phi_\kappa(x_i)$, as shown in Eq. (2b), which amplified the noise level in $\kappa(x_i)$. However, the $\mathrm{EDI}(x_i)$ signals constructed according to Eq. (2a), as presented in Fig. 6(b), (d) and (f), respectively, are still able to indicate the damage location with satisfactory accuracies, benefiting from the contributions from the $w_\kappa(x_i)$ signals (in Fig. 5(a)) in suppressing the random fluctuations in $\alpha\,\Phi_\kappa(x_i)$.

It is noteworthy that along with the increase of the severity and number of damage, as well as the level of noise influence, more random and fluctuated distribution of $Y(x_i)$ can be generated, compared with that shown in Fig. 5(b). Under such circumstance, *A* and *B* can still be estimated using liner curve fitting, with the exclusion of some outliers. The outliers were identified as the points of $Y(x_i)$ at a distance greater than a threshold (e.g., 2

standard deviation) from a baseline model, which is built using linear curve fitting based on the entirety of the data of $Y(x_i)$.

4. Experimental Validation

4.1 Setup

Experimental validation was carried out to further scrutinize the accuracy and robustness of the EPE in damage identification, by locating multiple cracks in a cantilever beam-like structure, as sketched in Fig. 7(a). The irregular shape of the structure, i.e., non-constant width near the free end, was intentionally designed to demonstrate the effectiveness of EPE subject to complex structural boundary geometries. The structure was made of aluminum 6061 with a density of 2.7 kg/m^3 and a Young's modulus of 68.9 GPa. The defined inspection region spanning over $[108\text{mm}, 476\text{mm}]$, shown in Fig. 7(a), features a constant width of 30mm and a uniform thickness of 8 mm, within which two through-width cracks (1.2mm×30mm× 2mm), each accounting for 0.2% of the beam-span, were pre-treated at 220mm and 380mm from the clamped end, respectively, as presented in Fig. 7(b). A harmonic excitation at 1000 Hz was applied on the beam with an electromechanical shaker (B&K®4809), near the free end of the structure. And 24 PZT sensors, with uniform diameters of 7 mm, were evenly attached on the intact surface of the structure within the inspection region, with identical adjacent distances to be 16 mm. As shown in Fig. 8(a), the voltage signal measured by the PZT sensors, proportional to dynamic strains (curvatures), was directly used to identify the cracks. In addition, vibration displacements were also measured using a SLV (Polytec® PSV-400B), as presented in Fig. 8(b). The distance between adjacent values of vibration displacements is 2 mm.

4.2 Identification Results Based on the Original PE and GSM

The original PE was first applied by using the displacements signal as shown in Fig. 8(b), according to a five-point finite difference scheme [1]. It can be seen in Fig. 8(c) that without any de-noising treatment, the identification result was excessively contaminated by measurement noise, unable to reflect any damage-related information.

The GSM was widely considered as a benchmark-free damage detection method depending on the approximation of curvature distribution using curve fitting techniques. So the measured signal in Fig. 8(a) was first used to construct the damage index of the GSM, expressed as

$$\mathrm{DI}_{GSM}\left(x_i\right)=\left|\kappa\left(x_i\right)-\kappa_{fit}\left(x_i\right)\right|, \tag{11}$$

where $\kappa\left(x_i\right)$ is the measured value and $\kappa_{fit}\left(x_i\right)$ is the approximated value. It should be noted that for the purpose of being compared with the damage index of EPE as shown in Eq. (2a), absolute value are used in Eq. (11), different from in other studies using square of the difference between measured and approximated values [20].

Because 1000 Hz is a relatively high frequency for the structure, i.e., between the 4th and 5th natural frequencies, Fourier series as shown in Eq. (9a) was still selected to approximate the strain/curvature distribution. By setting $n=4$, 6 and 8 in Eq. (9a), respectively, the approximated strain/curvature distribution was presented in Fig. 8(a), and the corresponding identification results constructed using Eq. (11) are shown in Fig. 9(a), (b) and (c), respectively.

4.3 Identification Results Based on the EPE

The damage index of the EPE, i.e., $\mathrm{EDI}(x_i)$, was constructed based on the signals of measured and approximated dynamic strains as shown in Fig. 8(a). According to $n=4$, 6 and 8 in Eq. 9(c), respectively, the re-constructed signals of vibration displacements basically coincide with each other, thus were represented by a single curve in Fig. 10. It should be noted that the displacements were re-constructed directly using the voltage signal as shown in Fig. 8(a), thus were with different scales compared with the measured data as shown in Fig. 8(b). Damage identification results of the EPE were presented in Fig. 11(a), (b) and (c), corresponding to $n=4$, 6 and 8 in Eq. (9c), respectively. It can be seen that although the two cracks are with same dimensions, the magnitudes of the damage indices of the EPE are different at the two crack locations, this is because of the difference of internal forces (i.e., bending moments and shear forces) at the two crack locations [1].

4.4 Discussion

Corresponding to a certain order of curve fitting, e.g., $n=6$ in Eq. (9c), the GSM is able to identify the crack locations with satisfactory accuracy, as shown in Fig. 9(b). However, the identification accuracy of the GSM shows high sensitivity to the variation of the order of curve fitting, by comparing Fig. 9(a), (b) and (c), probably resulting in poor identification accuracy due to improper order selection, as shown in Fig. 9(c). Compared with the GSM, superior stability and robustness of damage identification can be achieved by using EPE, as presented from Fig. 11(a) to (c), where the identification results show large similarity with each other, at the same time with high accuracy, although along with the variation of the order of curve fitting. The above difference between the GSM and EPE can be explained that: For the GSM, as shown in Eq. (11), the accuracy of curve fitting should be sufficiently high to approximate the global trend of the curvature/strain distribution, but

should not be “too high” to precisely depict the damage-induced singularity contained in the curvature distribution, as shown in Fig. 8(a) and 9(c) corresponding to $n=8$. Thus the order of curve fitting should be selected sophisticatedly for the GSM, to be neither too small nor too large. For the EPE, on the other hand, higher accuracy of curve fitting always leads to higher accuracy of displacements re-construction, due to the strict analytical relation between $\kappa(x)$ and $w_{\kappa}(x)$ as shown in Eq. (2c). And the local singularity contained in curvature distribution will be minimized in the re-constructed displacements, because of the integral operation of the curvature distribution, evidenced by comparing Fig. 8(a) and 10. It should be mentioned that for EPE, improved precision of damage identification can be achieved by increasing the density of measurement, which will naturally enhance the detection resolution and indicate the size of damage more accurately.

Another concern may be raised that compared with the GSM, the application of EPE requires additional information relating to structural geometry, material and vibration frequency, represented by different parameters as shown in Eq. (2b). Such a drawback can be overcome by setting α in Eq. (6b) as an additional unknown besides *A* and *B*. And *A*, *B* and α can be estimated by solving the combinations of the equations (as detailed in Section 2.2), as long as the number of equations (measurement points), i.e., *m* in Eq. (6b), is sufficiently large compared with the number of unknowns. By doing so, the reliance on the prior knowledge of the various parameters in Eq. (2b) can be prevented. Moreover, one of these parameters, e.g., E, can even be calculated according to Eq. (2b) using an estimated α, when other parameters are known.

5. Concluding Remarks

The effectiveness of EPE in damage identification, relying on the measurement of dynamic strains, was demonstrated in the present study. A statistical approach relying on curve fitting technique and structural local dynamic equilibrium was developed to re-construct the distribution of vibration displacements, by using the signal of measured curvature/strain. The damage identification results of EPE showed largely enhanced noise immunity compared with that of the original PE, and exhibited superior stability and robustness in damage identification compared with the GSM. Moreover, depending on a sufficiently large number of measurement points, the EPE was anticipated to be validly applied even without any prior knowledge of the basic parameters relating to structural geometry, martial and vibration frequency.

Depending on strain measurement, the EPE is able to perform on-line monitoring of structural health by using a wide range of types of strain sensors, showing potential of application in engineering practices, such as the monitoring of interfacial debonding for multi-layered civil structures [3]. In addition, the developed method also shows potential of identifying the location and magnitude of external force applied on tested structure. And under the case when damage and force coexist, they can be differentiated according to some unique signal features, for example, the detection results corresponding to damage exhibit drastic local oscillations, while those corresponding to external force do not show any oscillation. Relevant studies will be introduced in the future work.

Acknowledgements

This project is supported by National Natural Science Foundation of China (Grant No. 51375414 and 11272272). This project is also supported by the Hong Kong Research Grants Council via General Research Fund (GRF) (No. 15214414 and No. 523313).

References

[1]. H.Xu, L.Cheng, Z.Su and J.L.Guyader, Identification of damage in structural components based on locally perturbed dynamic equilibrium. Journal of Sound and Vibration 330 (24) (2011) 5963-5981.

[2]. H.Xu, L.Cheng, Z.Su and J.L.Guyader, Damage Visualization based on Local Dynamic Perturbation: Theory and Application to Characterization of Multi-damage in a Plane Structure. Journal of Sound and Vibration 332 (14) (2013) 3438-3462.

[3]. H.Xu, L.Cheng, Z.Su, J.L.Guyader and P.Hamelin, Reconstructing Interfacial Force Distribution for Identification of Multi-debonding in Steel-reinforced Concrete Structures Using Noncontact Laser Vibrometry. Structural Health Monitoring: An International Journal 12 (5-6) (2013) 507-521.

[4]. O.S.Salawu, Detection of Structural Damage Through Changes in Frequency: A Review. Engineering Structures 19 (9) (1997) 718-723.

[5]. Y.S.Lee and M.J.Chung, A Study on Crack Detection Using Eigenfrequency Test Data. Computers and Structures 77 (2000) 327-342.

[6]. X.Wang, N.Hu, H.Fukunaga and Z.H.Yao, Structural damage identification using static test data and changes in frequencies. Engineering Structures 23 (2001) 610-621.

[7]. N. Hu, X. Wang, H. Fukunaga, Z.H.Yao, H.X.Zhang and Z.S.Wu, Damage assessment of structures using modal test data. International Journal of Solids and Structures 38 (2001) 3111-3126.

[8]. A.Z.Khan, A.B.Stanbridge and D.J.Ewins, Detecting Damage in Vibrating Structures with a Scanning LDV. Optics and Lasers in Engineering 32 (2000) 583-592.

[9]. J.T.Kim, Y.S.Ryu, H.M.Cho and N.Stubbs, Damage Identification in Beam-type Structures: Frequency-based Method vs. Mode-shape-based Method. Engineering Structures 25 (2003) 57-67.

[10]. A.K.Pandey and M. Biswas, Damage Detection in Structures Using Changes in Flexibility. Journal of Sound and Vibration 169(1) (1994) 3-17.

[11]. Y.Aoki and O.Byon, Damage Detection of CFRP Pipes and Shells by Using Localized Flexibility Method. Advanced Composite Materials 10 (2001) 189-198.

[12]. G.Kawiecki, Modal damping measurement for damage detection. Smart Materials and Structures 10 (2001) 466-471.

[13]. M.S.Cao, W.Ostachowicz, R.B.Bai and M.Radzienski, Fractal mechanism for characterizing singularity of mode shape for damage detection. Applied Physics Letters 103 (2013) 221906.

[14]. M.S.Cao, W.Ostachowicz, M.Radzienski and W.Xu, Multiscale shear-strain gradient for detecting delamination in composite laminates. Applied Physics Letters 103 (2013) 101910.

[15]. J.-B.Ihn and F.-K.Chang, Pitch-catch active sensing methods in structural health monitoring for aircraft structures. Structural Health Monitoring: An International Journal 7 (2008) 5-19.

[16]. Z.Su, L.Ye and Y.Lu, Guided Lamb waves for identification of damage in composite structures: a review. Journal of Sound and Vibration 295 (2006) 753-780.

[17]. W.Ostachowicz, P.Kudela, P.Malinowski and T.Wandowski, Damage localisation in plate-like structures based on PZT sensors. Mechanical Systems and Signal Processing 23 (2009) 1805-1829.

[18]. K.Worden, C.R.Farrar, G.Manson and G.Park, The fundamental axioms of structural health monitoring. Proceedings of the Royal Society A 463 (2007) 1639-1664.

[19]. X.Zhao, H.Gao, G.Zhang, B.Ayhan, F.Yan, C.Kwan and J.L.Rose, Active health monitoring of an aircraft wing with embedded piezoelectric sensor/actuator network:

I. defect detection, localization and growth monitoring. Smart Materials and Structures 16 (2007) 1208-1217.

[20]. C.P.Ratcliffe and W.J.Bagaria, Vibration technique for locating delamination in a composite beam. AIAA Journal 36 (1998) 1074-1077.

[21]. P.Qiao, K.Lu, W.Lestari and J.L.Wang, Curvature mode shape-based damage detection in composite laminated plates. Composite Structures 80(2) (2007) 409-428.

[22]. A.K. Pandey, M. Biswas, M.M. Samman, Damage detection from changes in curvature mode shapes. Journal of Sound and Vibration 145(2) (1991) 321-332.

[23]. C.S.Hamey, W.Lestari, P.Qiao and G.Song, Experimental damage identification of carbon/epoxy composite beams using curvature mode shapes. Structural Health Monitoring: An International Journal 3(4) (2004) 333-353.

[24]. H.J.Lim, H.Sohn, M.P.DeSimio and K.Brown, Reference-free fatigue crack detection using nonlinear ultrasonic modulation under various temperature and loading conditions. Mechanical System and Signal Processing 45(2) (2014) 468-478.

[25]. E.O.Bayman, K.M.Chaloner, B.J.Hindman, M.M.Todd and the IHAST Investigators, Bayesian methods to determine performance differences and quantify variability among centers in multi-center trials: the IHAST trial. BMC Medical Research Methodology 13(5) (2013).

[26]. M.M.A.Wahab and G.D.Roeck, Damage detection in bridges using modal curvatures: application to a real damage scenario. Journal of Sound and Vibration 226(2) (1999) 217-235.

Table and Figure Captions

Table 1 Material properties and geometric parameters of the beam model for numerical validation

Figure 1 FE model of a cantilever beam bearing a damaged zone

Figure 2 (a) Distributions of curvature values calculated from FE analysis (i.e., $\kappa(x_i)$) and approximated using curve fitting (i.e., $\kappa_{fit}(x_i)$) according to $n=4$ in Eq. (9a), and (b) constructed signal of $\alpha\Phi(x_i)$ according to Eq. (8) based on $\kappa(x_i)$ as shown in (a)

Figure 3 (a) Distribution of $Y(x_i)$ calculated according to Eq. (6b) and the linear curve fitting based on the data of $Y(x_i)$, and (b) the re-constructed vibration displacements, compared with the true vibration displacements calculated based on FE analysis, in the absence of noise influence

Figure 4 Distribution of $\mathrm{EDI}(x_i)$ constructed according to Eq. (2a), in the absence of noise influence.

Figure 5 (a) Distributions of the true vibration displacements (calculated based on FE analysis without noise influence) and the re-constructed vibration displacements corresponding to $n=4$ in Eq. (9c), under noise influence with levels of being $\sigma(\varepsilon_i)=1\%$, 3% and 5% in Eq. (10), respectively, and (b) distribution of $Y(x_i)$ calculated according to Eq. (6b) subject to noise level of $\sigma(\varepsilon_i)=5\%$ and the linear curve fitting based on the noise-influenced data of $Y(x_i)$

Figure 6 Distributions of the absolute values of $\alpha\Phi(x_i)$ and $\mathrm{EDI}(x_i)$, subject to noise influence with levels of (a) and (b) $\sigma(\varepsilon_i)=1\%$, (c) and (d) $\sigma(\varepsilon_i)=3\%$, and (e) and (f) $\sigma(\varepsilon_i)=5\%$.

Figure 7 (a) Schematic of the damaged beam-like structure with multi cracks, and (b) image of the inspection region and the cracks

Figure 8 (a) Distributions of the voltage (strain) signal measured by PZT sensors and its approximations using curve fitting according to $n = 4$, 6 and 8 in Eq. (9a), respectively; (b) distribution of the vibration displacements measured by SLV, and (c) damage identification result of the original PE constructed using Eq. (1a) based on the measured vibration displacements shown in (b)

Figure 9 Damage identification results of the GSM constructed using Eq. (11), corresponding to (a) $n = 4$, (b) $n = 6$ and (c) $n = 8$ in Eq. (9a), respectively

Figure 10 Distribution of the re-constructed vibration displacements according to $n = 4$, 6 and 8 in Eq. (9c)

Figure 11 Damage identification results of the EPE constructed using Eq. (2a), corresponding to (a) $n = 4$, (b) $n = 6$ and (c) $n = 8$ in Eq. (9c), respectively

Table 1. Material and geometric properties of the simulated cantilever beam for numerical validation

Properties	Numerical value
Density ρ $\left[\mathrm{kg/m^3}\right]$	2700
Young's Modulus E $\left[\mathrm{GPa}\right]$	70
Beam length $L\left[\mathrm{mm}\right]$	1100
Width $b\left[\mathrm{mm}\right]$	10
Thickness $h\left[\mathrm{mm}\right]$	10

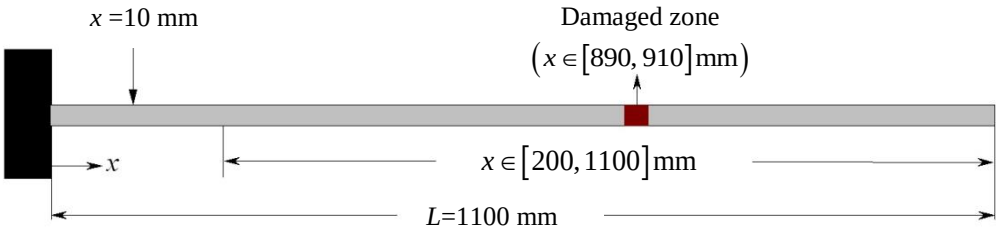

Figure 1

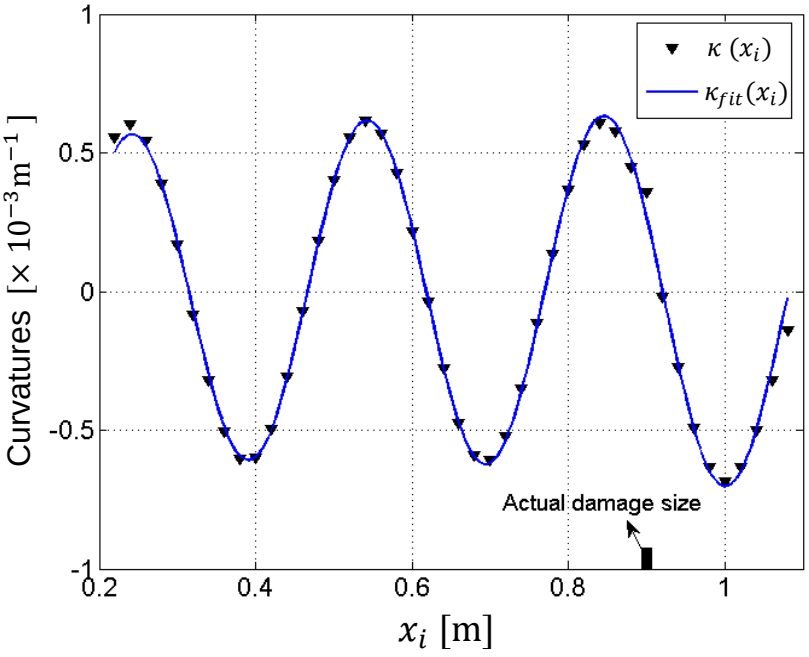
$\kappa\ (x_i)$
$\kappa_{fit}(x_i)$
Curvatures [$\times 10^{-3}$m^{-1}]
Actual damage size
x_i [m]

(a)

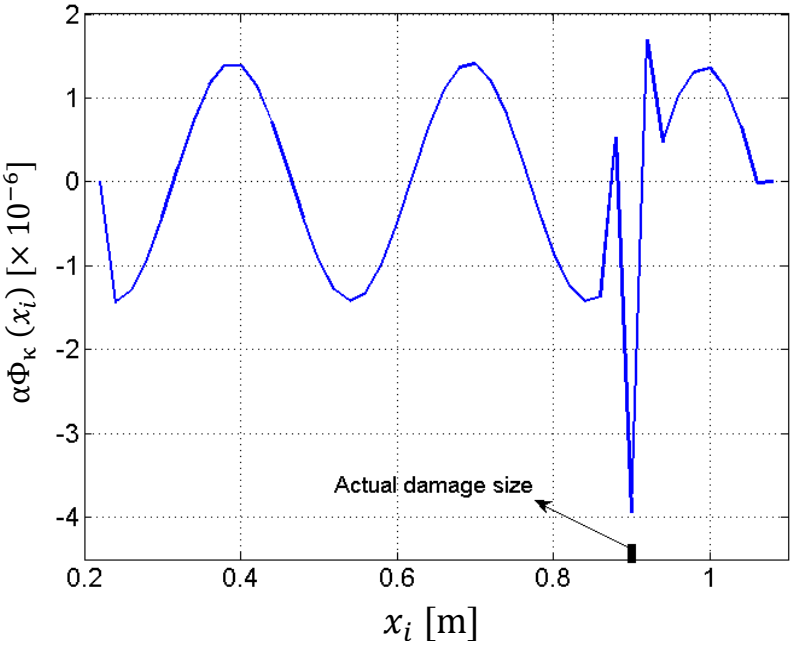
$\alpha\Phi_\kappa\ (x_i)$ [$\times 10^{-6}$]
Actual damage size
x_i [m]

(b)

Figure 2

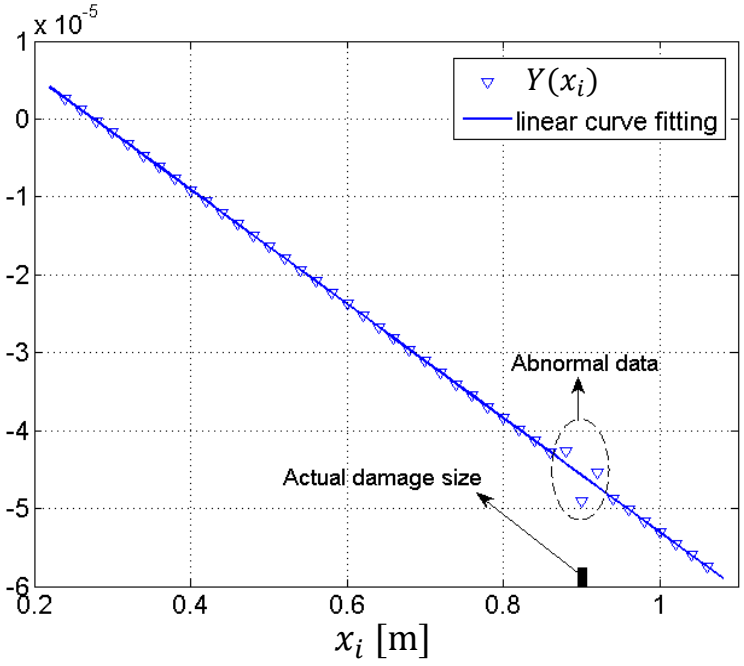
x 10^-5
1
0
-1
-2
-3
-4
-5
-6
0.2
0.4
0.6
0.8
1
$Y(x_i)$
linear curve fitting
Abnormal data
Actual damage size
x_i [m]

(a)

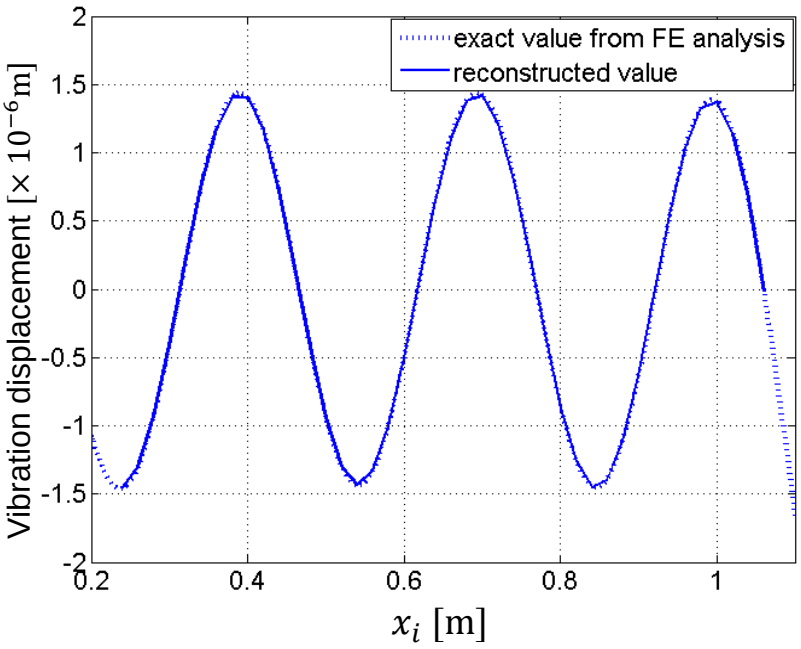
2
1.5
1
0.5
0
-0.5
-1
-1.5
-2
0.2
0.4
0.6
0.8
1
exact value from FE analysis
reconstructed value
Vibration displacement [× 10^{-6}m]
x_i [m]

(b)

Figure 3

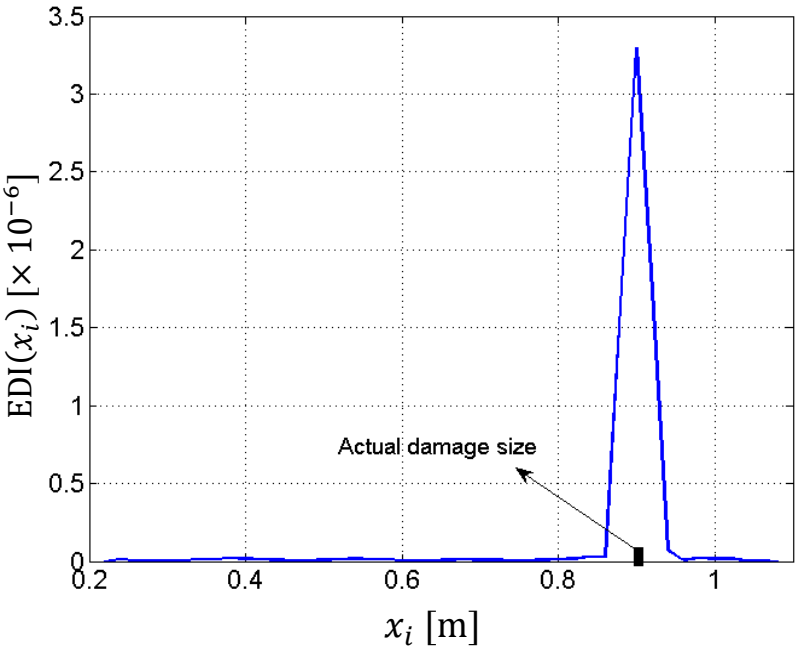
3.5
3
2.5
2
1.5
1
0.5
0
0.2
0.4
0.6
0.8
1
EDI(x_i) [$\times 10^{-6}$]
x_i [m]
Actual damage size

Figure 4

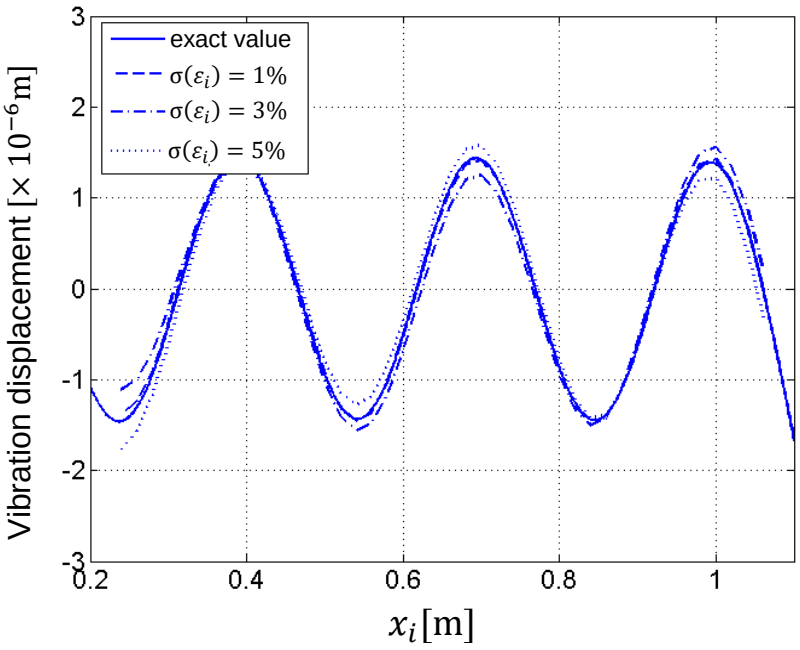
exact value
$\sigma(\varepsilon_i) = 1\%$
$\sigma(\varepsilon_i) = 3\%$
$\sigma(\varepsilon_i) = 5\%$
Vibration displacement [$\times 10^{-6}$m]
x_i[m]

(a)

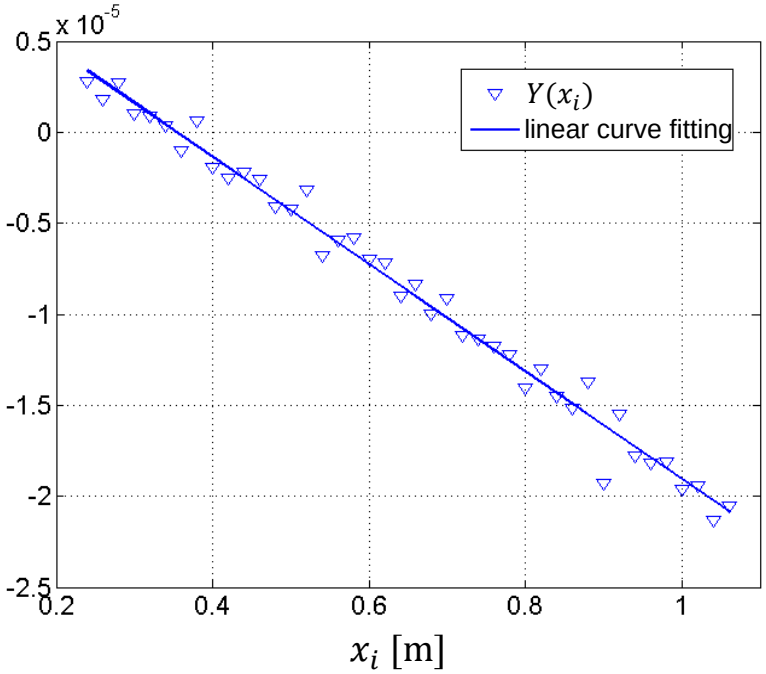
x 10^{-5}
$Y(x_i)$
linear curve fitting
x_i [m]

(b)

Figure 5

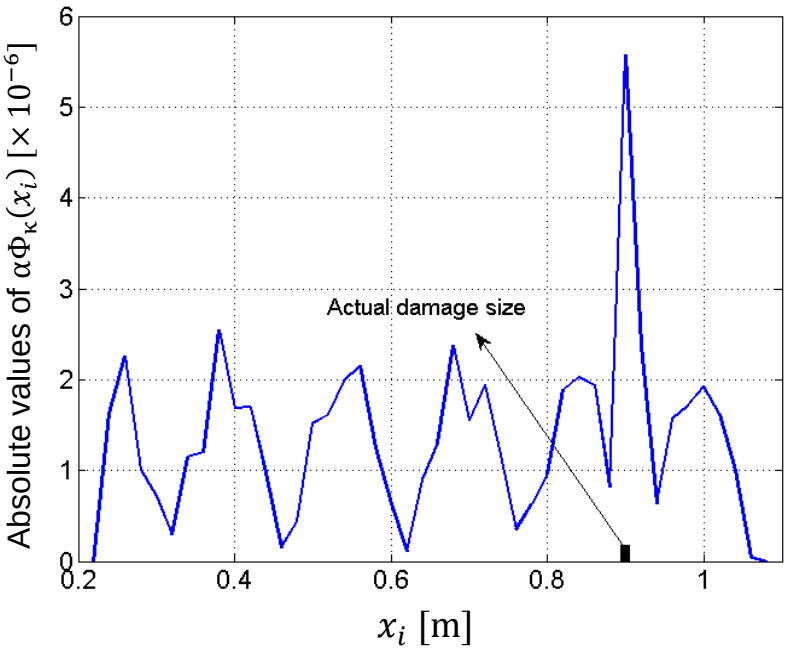
Absolute values of $\alpha\Phi_\kappa(x_i)$ $[\times 10^{-6}]$
Actual damage size
x_i [m]

(a)

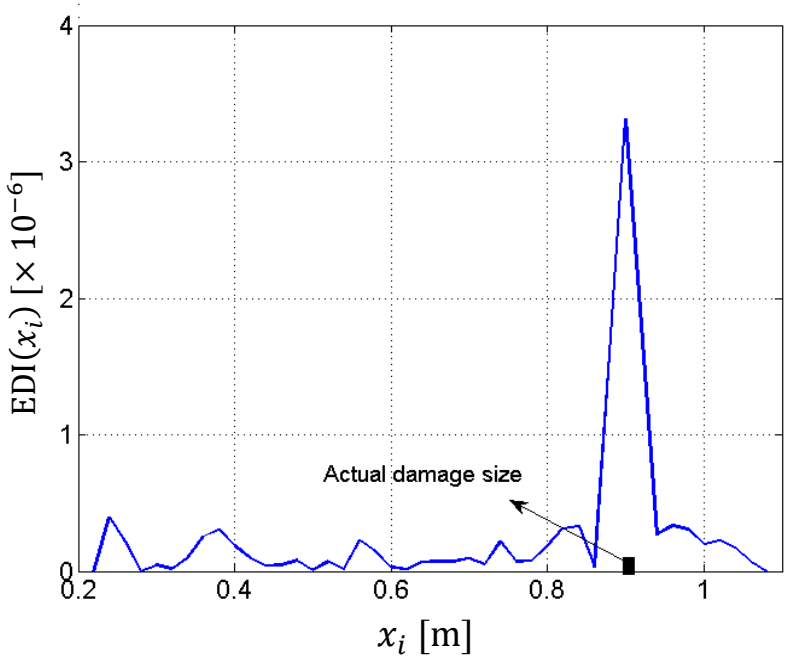
EDI(x_i) $[\times 10^{-6}]$
Actual damage size
x_i [m]

(b)

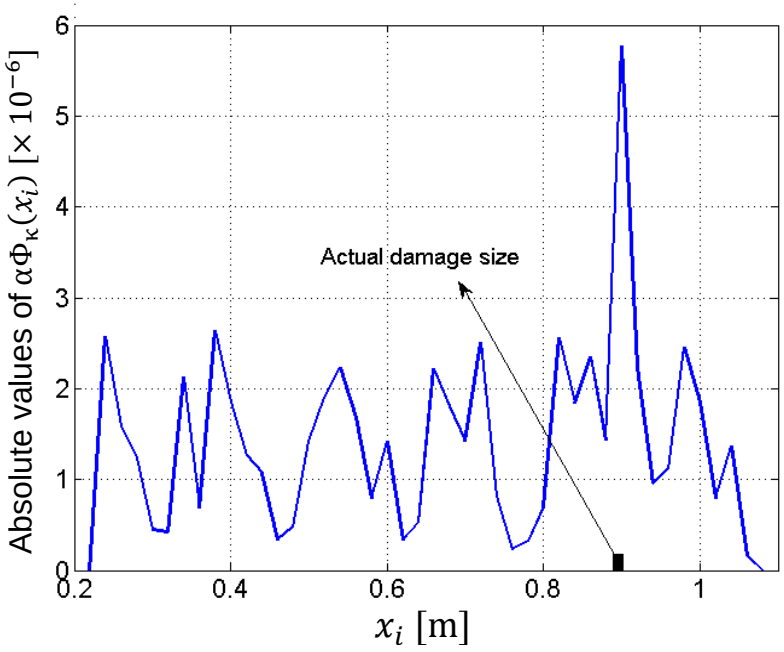
Absolute values of $\alpha\Phi_\kappa(x_i)$ [$\times 10^{-6}$]
Actual damage size
x_i [m]

(c)

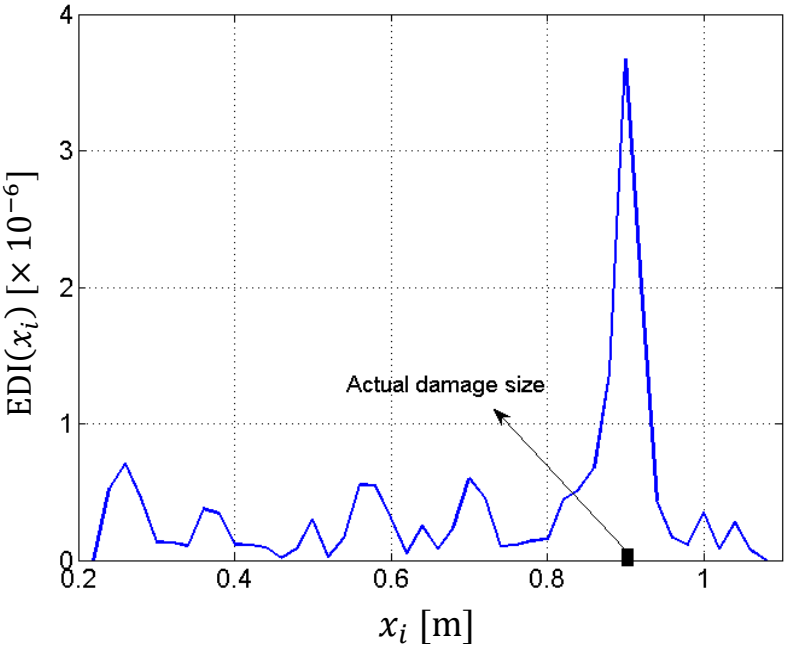
EDI(x_i) [$\times 10^{-6}$]
Actual damage size
x_i [m]

(d)

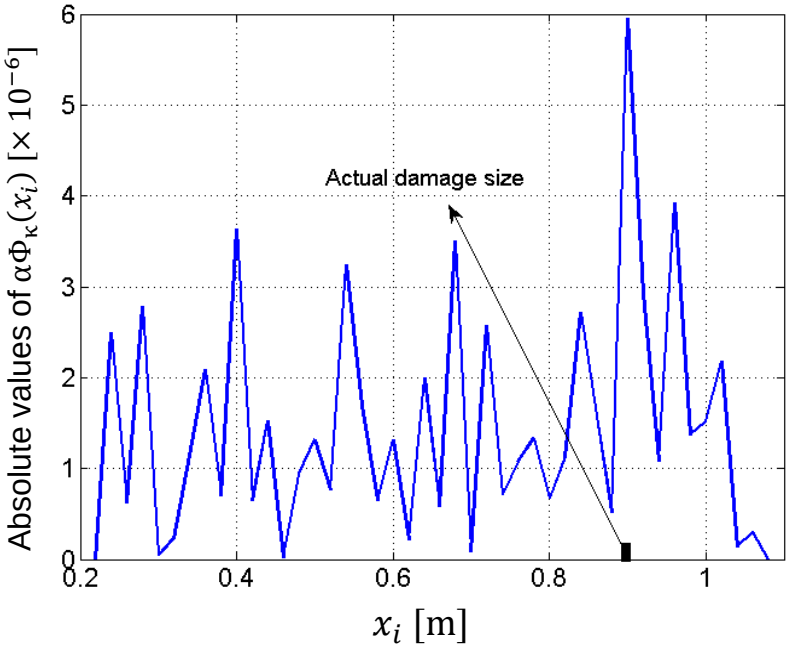
Absolute values of $\alpha\Phi_\kappa(x_i)$ $[\times 10^{-6}]$
Actual damage size
x_i [m]

(e)

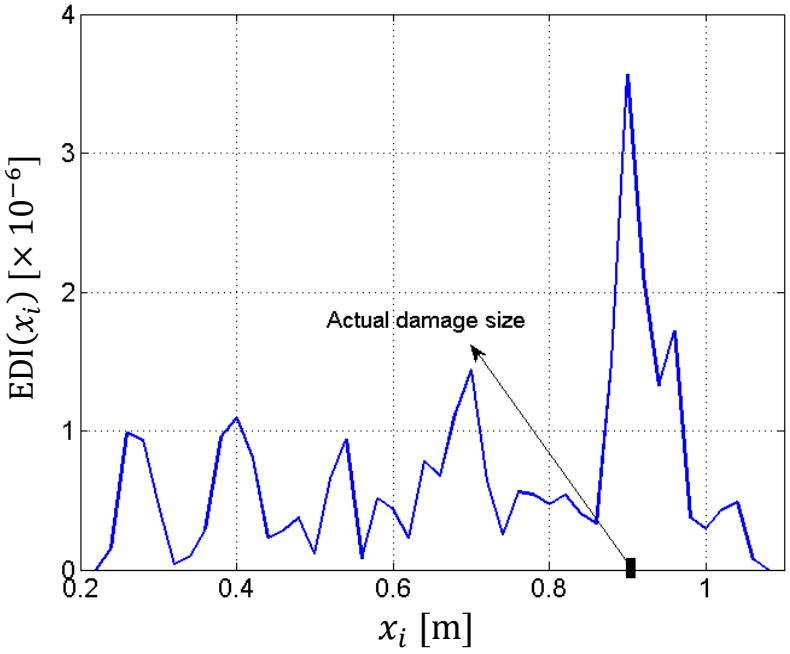
EDI(x_i) $[\times 10^{-6}]$
Actual damage size
x_i [m]

(f)

Figure 6

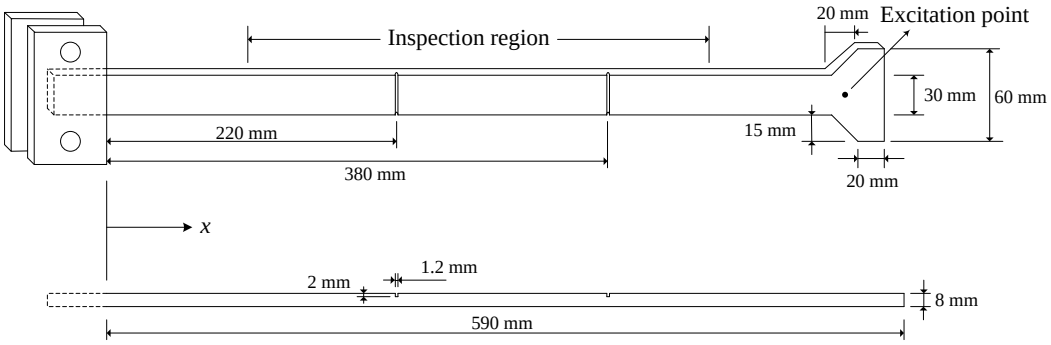
Inspection region
20 mm
Excitation point
30 mm
60 mm
220 mm
15 mm
380 mm
20 mm
x
1.2 mm
2 mm
8 mm
590 mm

(a)

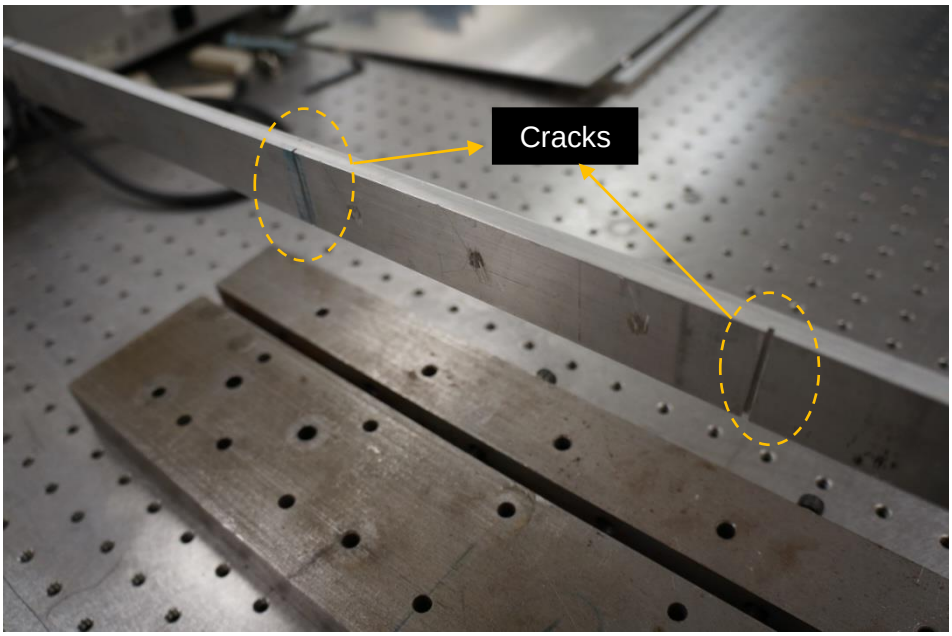
Cracks

(b)

Figure 7

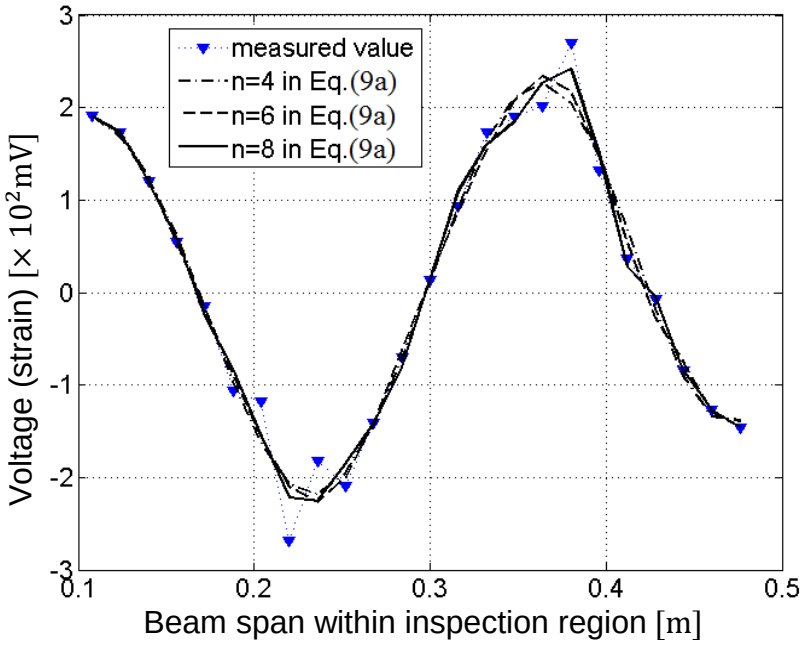
measured value
n=4 in Eq.(9a)
n=6 in Eq.(9a)
n=8 in Eq.(9a)
Voltage (strain) [× 10²mV]
Beam span within inspection region [m]
3
2
1
0
-1
-2
-3
0.1
0.2
0.3
0.4
0.5

(a)

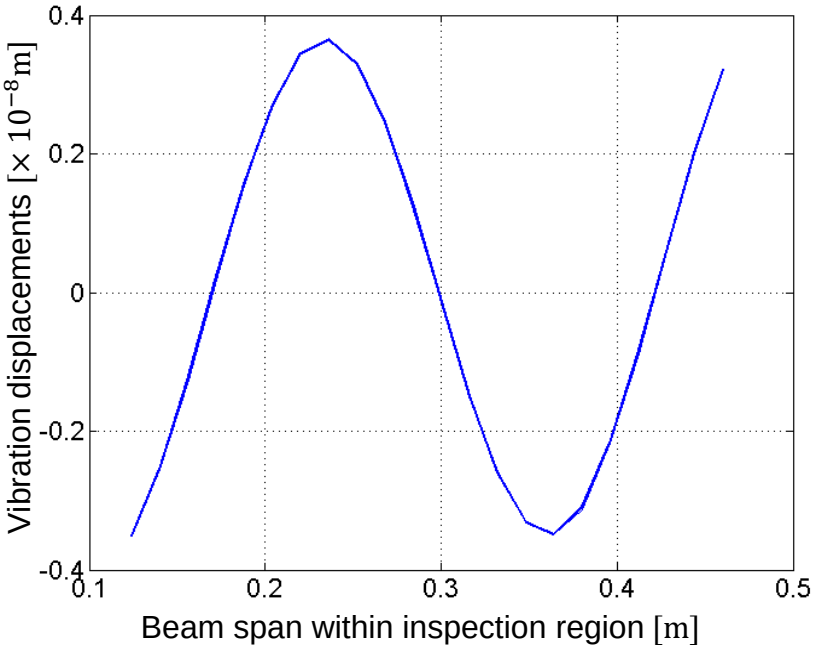
Vibration displacements [× 10⁻⁸m]
Beam span within inspection region [m]
0.4
0.2
0
-0.2
-0.4
0.1
0.2
0.3
0.4
0.5

(b)

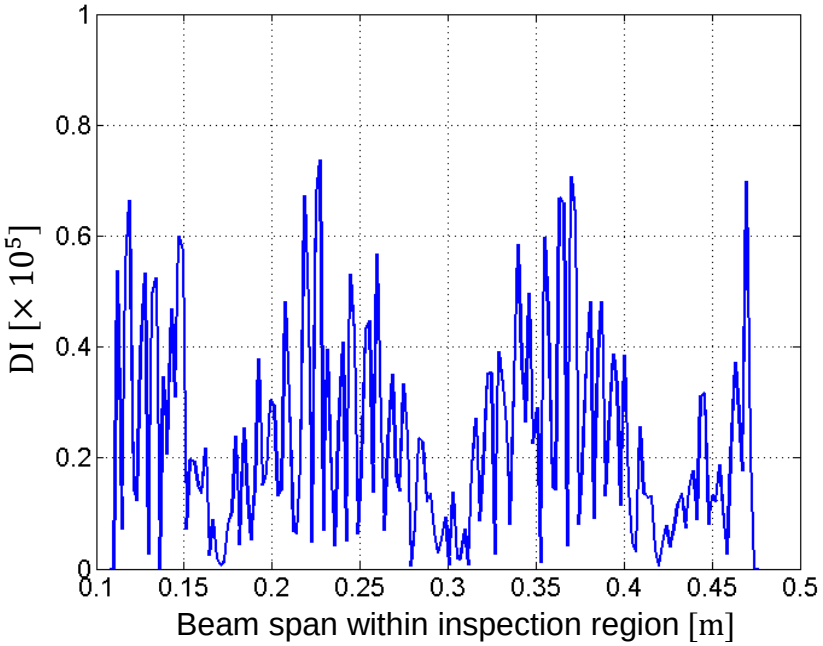
DI [× 10^5]
Beam span within inspection region [m]
0
0.2
0.4
0.6
0.8
1
0.1
0.15
0.2
0.25
0.3
0.35
0.4
0.45
0.5

(c)

Figure 8

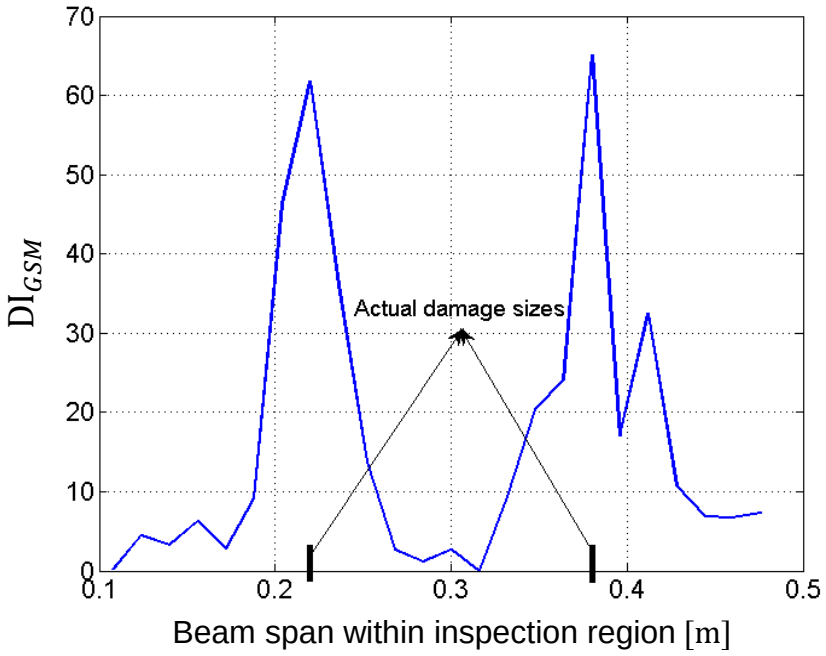
70
60
50
40
30
20
10
0
DI_{GSM}
Actual damage sizes
0.1
0.2
0.3
0.4
0.5
Beam span within inspection region [m]

(a)

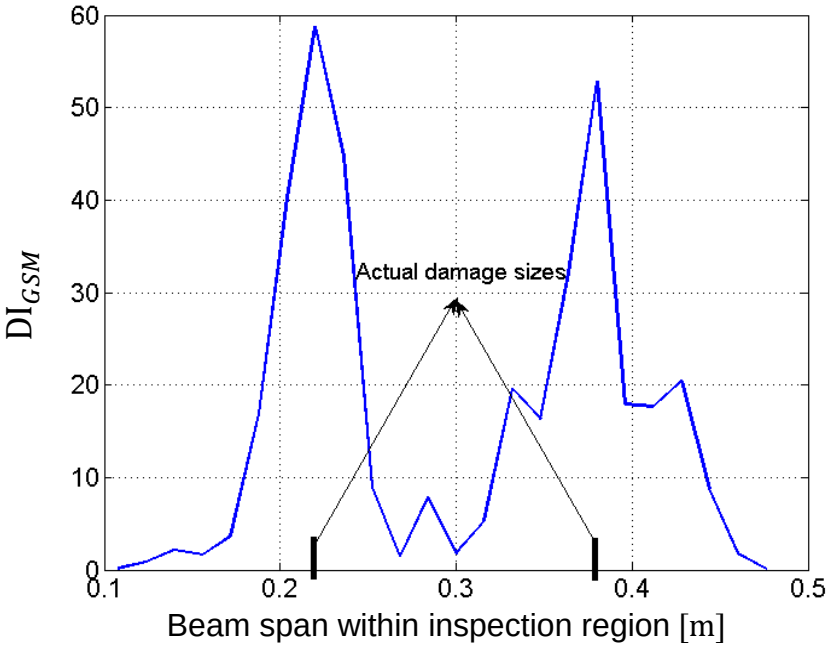
60
50
40
30
20
10
0
DI_{GSM}
Actual damage sizes
0.1
0.2
0.3
0.4
0.5
Beam span within inspection region [m]

(b)

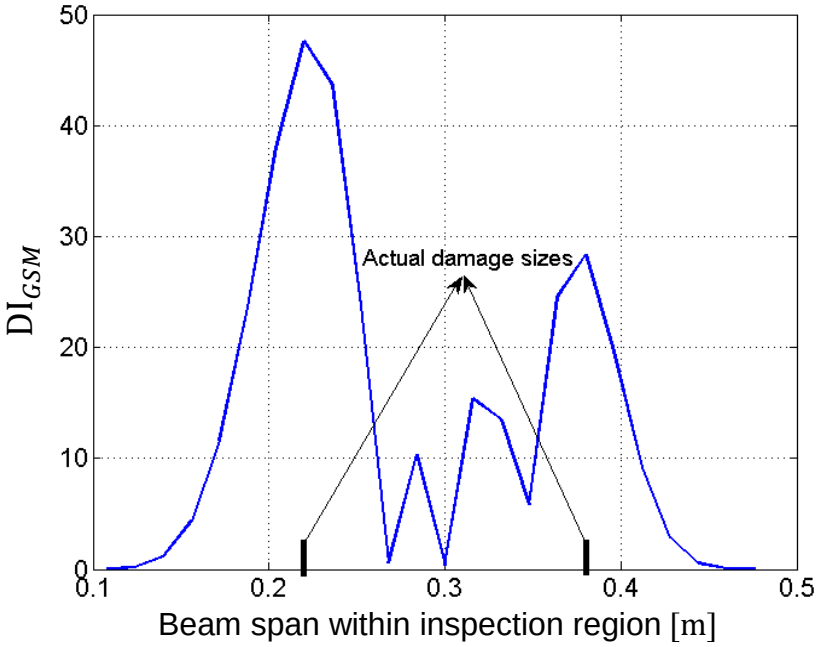
50
40
30
20
10
0
0.1
0.2
0.3
0.4
0.5
DI_{GSM}
Actual damage sizes
Beam span within inspection region [m]

(c)

Figure 9

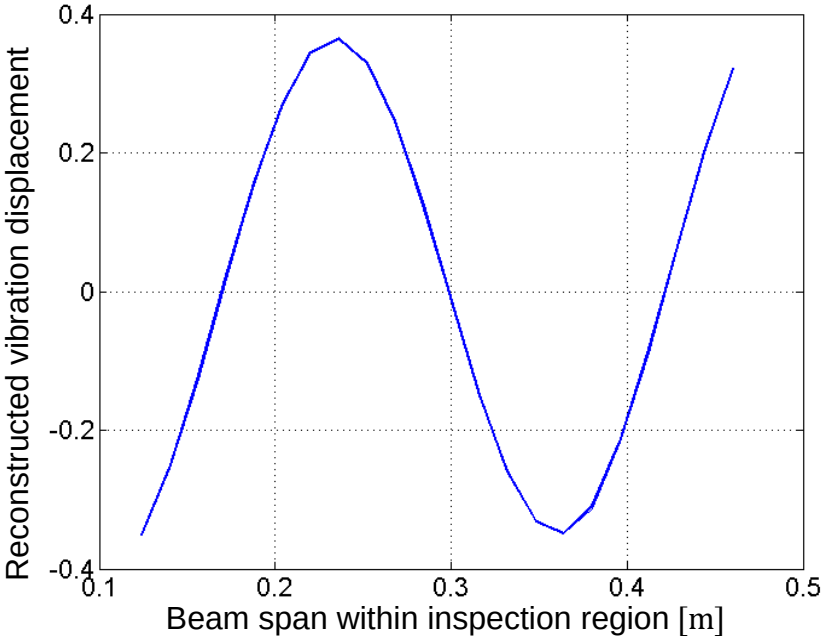
0.4
0.2
0
-0.2
-0.4
0.1
0.2
0.3
0.4
0.5
Reconstructed vibration displacement
Beam span within inspection region [m]

Figure 10

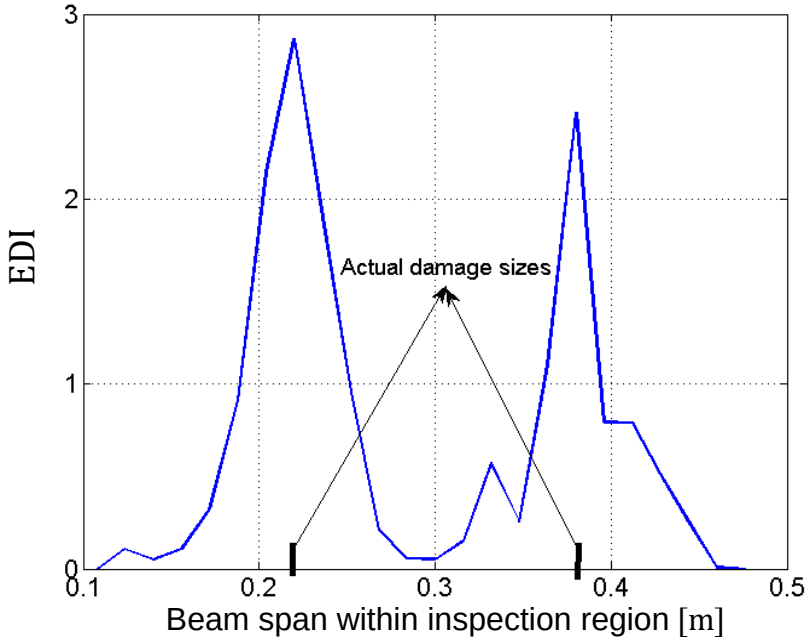
EDI
Actual damage sizes
Beam span within inspection region [m]
0
1
2
3
0.1
0.2
0.3
0.4
0.5

(a)

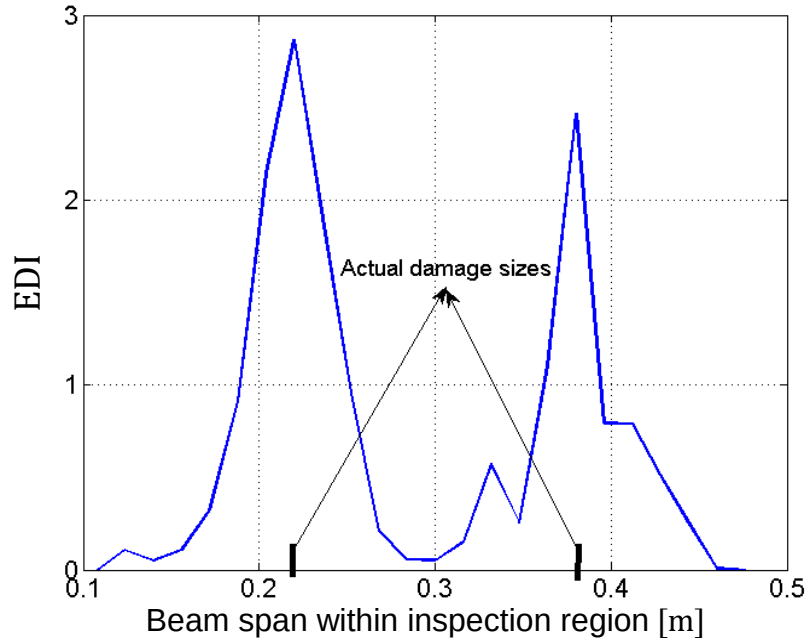
EDI
Actual damage sizes
Beam span within inspection region [m]
0
1
2
3
0.1
0.2
0.3
0.4
0.5

(b)

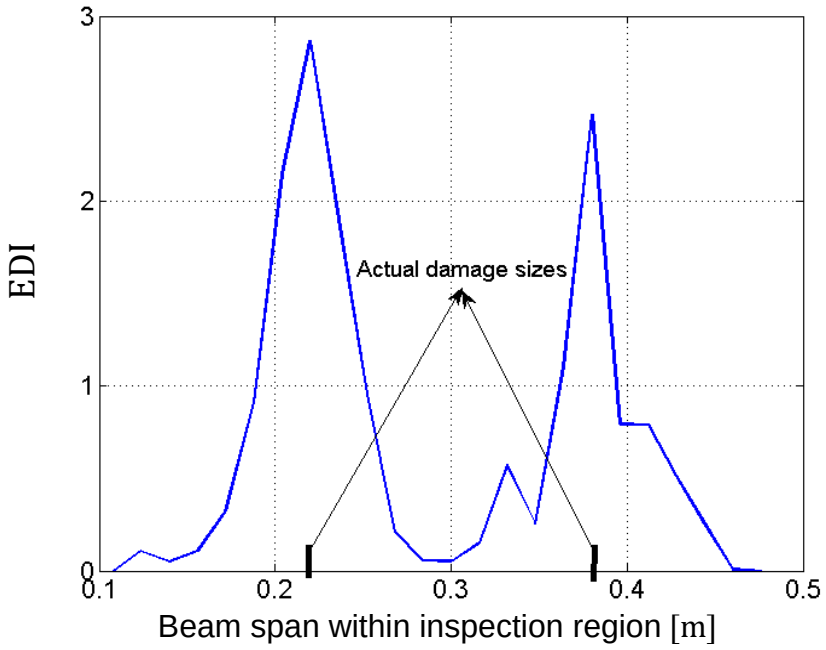
EDI
3
2
1
0
Actual damage sizes
0.1
0.2
0.3
0.4
0.5
Beam span within inspection region [m]

(c)

Figure 11